

**ANALYSIS ON THE INFLUENCE OF DIFFERENT FUEL COMBUSTION
HOT GASES ON THE COMBUSTOR CASING**

by

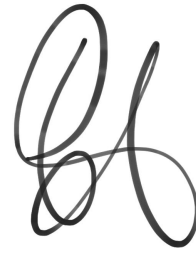
LIM BAN AIK

**This thesis submitted in fulfilment of the requirements for the
Bachelor Degree of Engineering (Honours) (Aerospace Engineering)**

July 2021

ENDORSEMENT

I, Lim Ban Aik hereby declare that all corrections and comments made by the supervisor and examiner have been taken consideration and rectified accordingly.



(Signature of Student)

Date: 11 July 2021



(Signature of Supervisor)

Name: Dr Nurul Musfirah Mazlan

Date: 11 July 2021



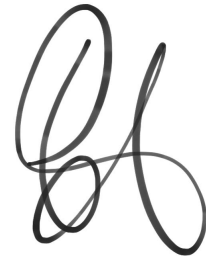
(Signature of Examiner)

Name: Ir. Dr. Hussin Mamat

Date: 11 July 2021

DECLARATION

This thesis is the results of my own investigation, except where otherwise stated and has not previously been accepted in substance for any degree and is not being concurrently submitted in candidature for any other degree.

A handwritten signature in black ink, consisting of a large, stylized 'H' with a loop at the top and a horizontal stroke at the bottom.

(Signature of Student)

Date: 11 July 2021

ACKNOWLEDGEMENT

First and foremost, I would like to express my deepest and sincere gratitude to my supervisor, Dr. Nurul Musfirah Mazlan, for her guidance, support, and encouragement during the completion of this research. Her professional guidance and countless advice have aided me in improving my engineering knowledge and gave me a lot of breakthroughs in this wonderful journey.

Besides, I would like to thank the technical support provided by the School of Aerospace Engineering, Universiti Sains Malaysia so we could access the computer in the CATIA Lab for simulation purpose that presented in this research.

In addition, I would also like to express my appreciation to the assistant engineer, Mrs. Rahayu, for always keeping up with us and solving technical issues we faced. Next, I would like to express my special thanks to the coursemates and friends who have given me suggestions and advices in completing this research.

Lastly, I would like to take this opportunity to express my gratefulness to my family and friends for their endless support throughout my whole undergraduate study.

Thank you.

ANALYSIS ON THE INFLUENCE OF DIFFERENT FUEL COMBUSTION HOT GASES ON THE COMBUSTOR CASING

ABSTRACT

In this modernized world, the aviation industry is growing drastically. Thus, much research is performed to improve aircraft performance. The most critical component to be designed is the gas turbine or specifically the combustor, as it needs to perform high-temperature combustion under a broad range of flight conditions. In order to study and optimize the performance of combustor, a computational method is called for. My project describes a simplified model of a combustor. The whole combustion chamber is modeled using SOLIDWORKS 2018. Subsequently, this project also presents a computational study of the flow field generated in the combustor and how that flow field convicts through the combustor. The fuels considered are Jet-A, Biodiesel, Camelina Bio-synthetic Paraffinic Kerosine (CSPK), and Ethanol. Another topic of interest is to perform the fluid-structure interaction (FSI) simulation to observe the effect of different fuels combustion on the mechanical properties of the combustor. All of these are simulated numerically through ANSYS 19.2 software. The result obtained show that the CSPK is the most optimized fuel. The results of FSI show that the structure deformation is small and negligible. Next, detectable plastic deformation occurs when the combustor is subjected to thermal stress, while plastic deformation is not notable when the combustor is subjected to pressure stress.

ANALYSIS ON THE INFLUENCE OF DIFFERENT FUEL COMBUSTION HOT GASES ON THE COMBUSTOR CASING

ABSTRAK

Dalam dunia moden ini, industri penerbangan berkembang secara drastik. Oleh itu, banyak kajian dilakukan untuk meningkatkan prestasi kapal terbang. Komponen yang paling kritikal untuk direkabentuk adalah turbin gas khususnya kebuk pembakaran, kerana ia perlu melakukan pembakaran yang melibatkan suhu tinggi dalam pelbagai keadaan penerbangan. Bagi mengkaji dan mengoptimumkan prestasi kebuk pembakaran, kaedah pengkomputeran diperlukan. Projek saya menerangkan model kebuk pembakaran yang dipermudahkan dan dimodelkan menggunakan SOLIDWORKS 2018. Seterusnya, projek ini juga menyajikan kajian komputasi medan aliran yang dihasilkan dalam kebuk pembakaran. Bahan bakar yang digunakan dalam projek ini adalah Jet-A, Biodiesel, Camelina Bio-synthetic Paraffinic Kerosine (CSPK), dan Ethanol. Topik yang seterusnya ialah mengaplikasikan simulasi interaksi bendalir-struktur (FSI) untuk memerhatikan kesan pembakaran bahan api yang berbeza terhadap sifat mekanik pembakar. Semua ini disimulasikan secara dengan menggunakan perisian ANSYS 19.2. Hasil kajian yang diperolehi menunjukkan bahawa CSPK adalah bahan bakar yang paling dioptimumkan. Hasil kajian FSI pula menunjukkan bahawa deformasi bentuk struktur adalah kecil dan boleh diabaikan. Seterusnya, deformasi plastik yang agak jelas berlaku apabila kebuk pembakaran mengalami tekanan haba, sementara deformasi plastik boleh diabaikan apabila kebuk pembakaran mengalami tekanan beban.

TABLE OF CONTENTS

ENDORSEMENT	i
DECLARATION	ii
ACKNOWLEDGEMENT	iii
ABSTRACT	iv
ABSTRAK	v
TABLE OF CONTENTS	vi
LIST OF FIGURES	viii
LIST OF TABLES	x
LIST OF ABBREVIATIONS	xi
LIST OF SYMBOLS	xii
CHAPTER 1 INTRODUCTION	1
1.1 Overview	1
1.2 Problem Statement	2
1.3 Research Objectives	3
1.4 Research Scope	3
1.5 Thesis Outline	3
CHAPTER 2 LITERATURE REVIEW	5
2.1 Overview	5
2.2 Combustion Simulation	6
2.3 Failure Analysis	8
2.4 Computational Fluid Dynamics	9
2.4.1 Species Transport Equation	9
2.4.2 Energy Equation	10
2.4.3 Eddy-Dissipation Model	10
2.4.4 Standard $k - \epsilon$ model	11
2.4.5 Standard $k - \omega$ model	12
2.4.6 Shear-Stress Transport (SST) $k - \omega$ model	12
2.4.7 Selection of turbulence model	13
2.5 Fluid-Structure Interaction	13
2.6 Research Gap	14
CHAPTER 3 METHODOLOGY	16
3.1 Overview	16
3.2 Geometry Selection of combustor	17

3.2.1	Casing Area	20
3.2.2	Diffuser Dimension	21
3.2.3	Swirler Dimensions	22
3.2.4	Recirculation Zone Dimensions	23
3.3	Fluid Domain Solver Setup	24
3.4	Structure Domain Solver Setup	26
3.5	Grid Independence Test	29
3.5.1	Fluid Domain	29
3.5.2	Structure Domain	32
3.6	Validation	34
CHAPTER 4 RESULTS AND DISCUSSION		36
4.1	Geometry of the Combustor	36
4.2	Combustion Performance of the Fuel	38
4.3	Fluid-Structure Interaction	46
CHAPTER 5 CONCLUSIONS AND FUTURE WORKS		58
5.1	Conclusions	58
5.2	Future Works	59
REFERENCES		60

LIST OF FIGURES

Figure 2.1: Combustor geometry with no cooling holes(Adhikari, 2016)	6
Figure 2.2: Combustor geometry with film cooling(Adhikari, 2016)	7
Figure 2.3: Combustor geometry with effusion cooling hole(Adhikari, 2016)	7
Figure 3.1: General flowchart of this research	16
Figure 3.2: Detailed flowchart for simulation process	17
Figure 3.3: Preliminary design procedure of the combustor (Mark and Selwyn, 2016)	18
Figure 3.4: Reference length D_{ref} for tubular combustor (Conrado <i>et al.</i> , 2004)	20
Figure 3.5: One-way FSI setup for pressure stress and thermal stress	26
Figure 3.6: The FEA model of the combustor	27
Figure 3.7: Strength to weight ratio of material	27
Figure 3.8: Fix support on the combustor	28
Figure 3.9: Fluid Domain Grid Independence Test	30
Figure 3.10: Meshing of the fluid domain	31
Figure 3.11: Named selection for boundary condition	31
Figure 3.12: Structure Domain Grid Independence Test	33
Figure 3.13: Structure mesh	34
Figure 3.14: Average outlet temperature	35
Figure 4.1: Main configuration of the combustor	37
Figure 4.2: CAD model of the combustor	38

Figure 4.3: Pressure contour on the midplane (a) Jet-A (b) Biodiesel (c) CSPK (d) Ethanol	40
Figure 4.4: Velocity contour on the midplane (a) Jet-A (b) Biodiesel (c) CSPK (d) Ethanol	42
Figure 4.5: Temperature contour on the midplane (a) Jet-A (b) Biodiesel (c) CSPK (d) Ethanol	44
Figure 4.6: Pressure acting on the combustor casing (a) Jet-A (b) Biodiesel (c) CSPK (d) Ethanol	46
Figure 4.7: Temperature acting on the combustor casing (a) Jet-A (b) Biodiesel (c) CSPK (d) Ethanol	47
Figure 4.8: Total deformation of the combustor casing (a) Jet-A (b) Biodiesel (c) CSPK (d) Ethanol	49
Figure 4.9: Equivalent von Mises stress in the combustor by pressure load and thermal load (a) Jet-A (b) Biodiesel (c) CSPK (d) Ethanol	52
Figure 4.10: Equivalent von Mises elastic strain of the combustor by pressure load and thermal load (a) Jet-A (b) Biodiesel (c) CSPK (d) Ethanol	53
Figure 4.11: Graph of yield strength comparison	56

LIST OF TABLES

Table 3.1: Typical values used in combustor	19
Table 3.2: Operating condition for calculation process and simulation (Luis Goular Dias, Antonio Rosa do Nascimento and de Oliveira Rodrigues, 2014)	19
Table 3.3: Fuel Properties	24
Table 3.4: Solver setup and boundary condition	24
Table 3.5: Material properties of aluminum	28
Table 3.6: Table of GIT (Fluid Domain)	30
Table 3.7: Table of GIT (Structure Domain)	33
Table 4.1: Detailed dimension of the combustor casing	36
Table 4.2: Thrust produces by each fuel	45
Table 4.3: Maximum equivalent von Mises stress and elastic strain by pressure load and thermal load	55

LIST OF ABBREVIATIONS

CFD	: Computational Fluid Dynamics
GIT	: Grid Independence Test
RANS	: Reynolds Averaged Navier-Stokes
SST	: Shear Stress Transport
CAD	Computer-aid design
FSI	fluid-structure interaction
FEA	Finite element analysis
CSPK	Camelina Bio-synthetic Paraffinic Kerosine

LIST OF SYMBOLS

A_{ref}	: Reference area
$\Delta P_{3-4}/P_3$: Total pressure loss
$\Delta P_{3-4}/q_{ref}$: Function of the pattern factor
D_{ref}	: Reference diameter
D_L	: Liner diameter
A_L	: Liner area
A_{an}	: Annulus area
PF	: Pattern factor
T_{max}	: Maximum exit temperature
L_L	: Liner length
L_{PZ}	: Primary zone length
L_{SZ}	: Secondary zone length
L_{DZ}	: Dilution zone length
A_o	: Snout outer area
\dot{m}_3	: Inlet air mass flow rate
\dot{m}_{an}	: Annulus air mass flow rate
D_o	: Snout outer diameter
φ	: Diffuser angle
L_{dif}	: Diffuser length
A_s	: Snout area
\dot{m}_{RZ}	: Recirculation zone mass flow inlet
C_{ds}	: Snout discharge coefficient

D_s	: Snout diameter
A_{sw}	: Swirler flow area
K_{sw}	: Concordance factor
β_{sw}	: Turning angle
D_{sw}	: Swirler diameter
D_{hub}	: Injector hub diameter
n_B	: Number of swirler blades
L_{RZ}	: Recirculation zone length
θ_{RZ}	: Recirculation zone angle
L_{dome}	: Dome length
R_i	: Net rate of production species
S_i	: Rate of creation
J_i	: Diffusion flux
$D_{i,m}$: Mass diffusion coefficient
Sc_t	: Turbulent Schmidt number
μ_t	: Turbulent viscosity
k	: Thermal conductivity
T	: Temperature
S_{rad}	: Radiative source term
S_h	: Chemical source term
h_j^0	: Enthalpy of formation
R_j	: Volumetric rate of creation
$R_{i,r}$: Species production net rate
G_k	: Generation of turbulence kinetic energy
Y_M	: Contribution of the fluctuating dilatation

S_k, S_ε	: User-defined source terms
$C_{1\varepsilon}$: Constant
$C_{2\varepsilon}$: Constant
$C_{3\varepsilon}$: Constant
σ_k	: Turbulent Prandtl numbers for k
σ_ε	: Turbulent Prandtl numbers for ε
G_ω	: Generation of specific dissipation rate
Y_k	: Dissipation of k
Y_ω	: Dissipation of ω
Γ_k	: Effective diffusivity of k
Γ_ω	: Effective diffusivity of ω
\widetilde{G}_k	: Generation of turbulence kinetic energy
D_ω	: Cross-diffusion form

CHAPTER 1

INTRODUCTION

1.1 Overview

The gas turbine combustion chamber is one of the most crucial components to be developed because it must assure stable functioning in a wide range of air to fuel ratios and high temperature. So, a gas turbine combustor is typically a device to raise the temperature of the incoming air stream from the compressor by the additional injection and combustion of the fuel. Noted that the combustion process is a complex phenomenon involving fluid dynamics and chemical kinetics that occurs within the confines of the combustor's limited volume. Furthermore, proper combustion is critical for improving total combustor efficiency.

Other than that, the combustor can also be described as an essential hot end component of an aero-engine, of which the reliability has a direct impact on the operation safety of the aircraft. Thus, the combustor must fulfill numerous requirements, such as initiating ignition efficiently and operating stably over various conditions.

Besides, it is expected to provide complete combustion of the fuel at all operating conditions while reducing undesirable pollutants. A good mix of air and fuel is also vital to obtain a uniform exit temperature distribution to avoid damaging the turbine. Thus, designing a combustor is not an easy task as it needs to fulfill the requirements mentioned, so the compacted configuration of the combustor with high reliability, minimum size, weight, and the cost is a great challenge to be achieved.

Therefore, this paper will present a CAD model designed with the designation process by (Conrado *et al.*, 2004). This paper will also give a detailed CFD simulation of the designed combustor about the combustion characteristic of Jet-A, CSPK, Biodiesel, and Ethanol along with the integration of FSI analysis to study the mechanical properties behaviour of the combustor.

1.2 Problem Statement

It is well known that a combustor is a component that constantly works under high temperature, high stress, high corrosion loads, and high pressure, which leads to various types of failure due to different causes. So, the main challenge for the combustor would be finding an optimized design that suits the necessity of both mechanical and combustion performance.

For many years to come, the combustion of fossil fuels releases pollutants that, if left unchecked, will cause a variety of issues such as the greenhouse effect and ozone depletion. Hence, the demand for clean and reliable power is a potential solution to the massive pollution problems when many countries impose strict environmental issues. So, alternative fuel like biofuel, syngas fuels is slowly adapted into the industrials. Instead of repeating the research done by other researchers where it is only focused on reducing the emission of pollutants, this paper will discuss the effect of fuel properties differently, which is the effect of the alternative fuel properties on the mechanical properties of the combustor.

1.3 Research Objectives

The objectives of this thesis are:

1. Examine the combustion characteristics of four different fuel types, including Jet A, CSPK, Biodiesel, and Ethanol.
2. Evaluate the mechanical properties, including total deformation, stress, and strain of the combustor casing using fluid-structure interaction (FSI).

1.4 Research Scope

The study herein is purely a numerical simulation work as the first approach to study the fuel combustion effect on the combustor casing, without considering the emission of pollutant and the variation of the combustor type. There will not be hands-on experimental work conducted in the laboratory. Only the cruising phase is considered for the combustion performance evaluation. Besides, the flow is deemed to be turbulent inside the combustor, and no heat transfer is considered. The main focus will be on weight reduction from the aspect of material selection, and then it will be imported for the FSI simulation.

1.5 Thesis Outline

Chapter 1 is about the introduction on the brief explanation about combustor and the highlights of this study that include the problem statement, objectives, and research scope. Chapter 2 is about the findings on the relevant studies carried out in the past on combustion performance, experimental work, numerical approach, FSI, designation process of the combustor. While Chapter 3 is about the methodology carried out to reach

the study objectives. In this chapter, the approaches are divided into geometry selection for the combustor, one-way FSI, solver setup, validation process, and grid independence test. Then, in Chapter 4, the results from the methodology are presented and discussed. Finally, the study is concluded with the significant findings and future works recommendations in Chapter 5.

CHAPTER 2

LITERATURE REVIEW

2.1 Overview

Despite the variation and advancement in the combustor design, the challenge to the inventiveness and creativity in the designing process is significantly more remarkable since the new concepts and technology are needed to satisfy the projected emission and provide energy conservation. Besides, the combustor is an essential component in the gas turbine which all the multiphase chemical kinetic, evaporation, combustion, and heat transfer processes occur.

According to (Gupta, 1997), due to the gradual deterioration in the air quality and the greenhouse effect, reduction of pollutant emission and combustion efficiency became the priority of design requirement. As a result, the development process will require a detailed understanding of the advanced design concept and advanced cooling configuration to improve the combustor geometrically and combustion efficiency within the acceptable range of pressure loss and achieving a more uniform temperature distribution within the combustor.

To enhance the overall performance and reliability of the combustor liner, quite a few studies have been made by manipulating the geometry parameter, analyzing the effect combustion performance in the combustor, and the failure analysis on the combustor casing to study and understand the flame stability and distribution, failure mode of the casing and pollutant emission in order to manufacture an optimized combustor that suits a wide range of use in the aerospace industry and looking forward to prolonging the combustor's service life.

2.2 Combustion Simulation

(Luis Goular Dias, Antonio Rosa do Nascimento and de Oliveira Rodrigues, 2014) presented the investigation of the velocity profile and temperature distribution under the influence of the reference area as it is the prime physical parameter that affects the other dimension like the liner area, diffuser length, snout diameter, etc. The numerical analyses were performed using the ANSYS software. The finding concluded that the methodology and model equations developed by (Lefebvre, 2010) are suitable. However, the velocity flow field in the combustor is still high, which worsens the mixing of the fuel and the air, thus increasing the emission of the pollutant. After modifying the geometry by increasing the reference area, the improvement of the combustion process can be observed by reducing the burning rate in the combustion region.

(Adhikari, 2016) conducted a study regarding the effect of the cooling hole on the combustion performance to obtain the desired optimum temperature gradient to alleviate the effect of the hot combusted gas on the wall of the combustor. In the study, the CFD software ANSYS Fluent was used to demonstrate the impact of the cooling slots.

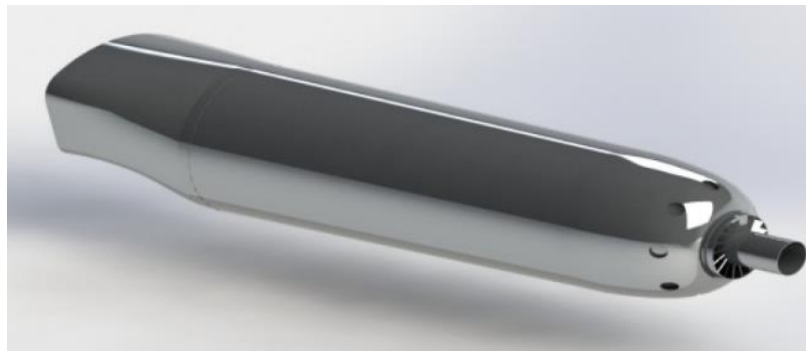


Figure 2.1: Combustor geometry with no cooling holes(Adhikari, 2016)

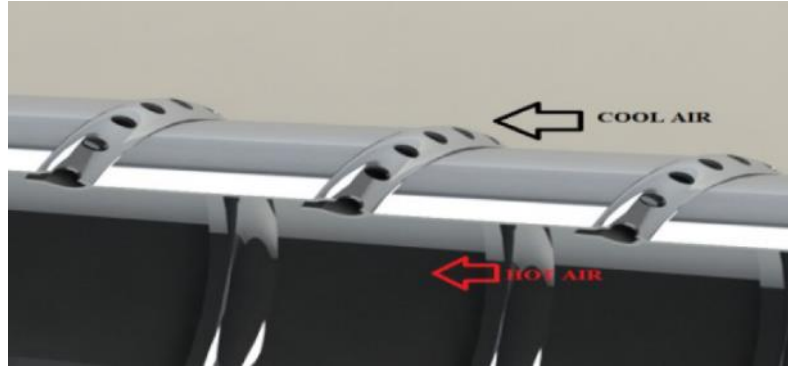


Figure 2.2: Combustor geometry with film cooling(Adhikari, 2016)

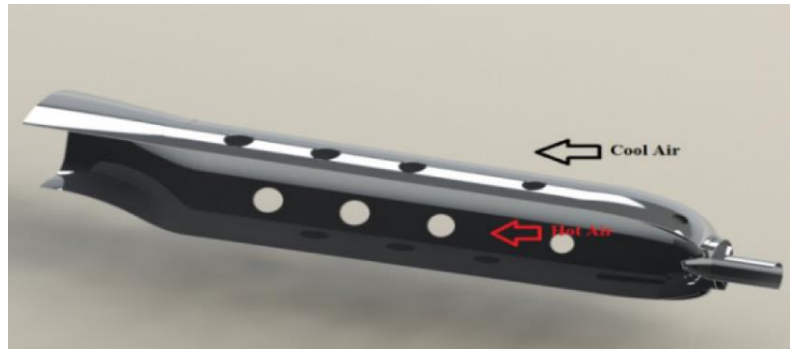


Figure 2.3: Combustor geometry with effusion cooling hole(Adhikari, 2016)

The result showed that the combustor with no cooling holes has poor combustion performance due to the lack of primary air for the combustion enhancement; hence, complete combustion did not occur. The combustion of the combustor with film cooling holes was promising as it improves the surface cooling because the combustion only took place and propagate along the center region. The last analysis was about the combustor with effusion cooling holes; the cooling effect provided by the effusion cooling holes was presented on the combustor walls, which reduced the temperature progressively. The difference between the film cooling is that the flame was spreading toward the wall. The effusion cooling is found to lower the temperature of the hot gas. Conclusively, the film

cooling and effusion cooling in the geometry designation process will result in symmetric temperature distribution and boost the flame stability.

2.3 Failure Analysis

In the past decade, many researchers have done numerous works on aero-engine combustor failure analysis. (Lv, Li and Fu, 2010; Zhang *et al.*, 2020) carried out the macroscopic and microscopic observation and chemical analysis to study the damage, failure, and crack of an aero-engine combustor liner. The results show that high-temperature ablation and thermal fatigue crack cause the notches failure modes, axial directional crack along the combustor, and crack at the edge near the weld spot. Another meaningful information extracted is the primary reason for the ablation failure, and the crack is due to the lousy configuration of the crossover tube. So, to avoid any similar failure, the satisfactory desire could be to enhance the design of the crossover tube or provide a reparative measure.

On the other hand, (Naraparaju *et al.*, 2014) performed a study on an aero-engine combustor thermal barrier coating (TBC) after the service in the sand attack region. To examine the microstructural change of the test sample, scanning electron microscopy and X-ray diffractometry were applied. The results show that the main damage pattern of the combustor TBC is the CMAS damage pattern. Besides, (Wang, Zhang and Tan, 2012) show that the poor quality of the roll welding seam is the leading cause of the explosion of a combustor shell failure which leads to a failure by performing the metallographic analysis and mechanical calculation.

2.4 Computational Fluid Dynamics

The branch of fluid mechanics that solves and analyzes fluid flow problems using numerical approaches are referred to as computational fluid dynamics (CFD). CFD is broadly applied in research and engineering problems of various fields of study as well as industries. This current study utilizes the available commercial CFD code ANSYS Fluent to simulate the fluid flow inside the combustor and ANSYS Mechanical for the FEA simulation.

2.4.1 Species Transport Equation

The masses of the different chemical species are conserved like the overall mass. The FLUENT predict the local mass fraction of each species, Y_i , through the solution of a convection-diffusion equation for the i^{th} species. The equation of conservation is:

$$\frac{\partial}{\partial t}(\rho Y_i) + \nabla \cdot (\rho \vec{v} Y_i) = -\nabla \cdot \vec{J}_i + R_i + S_i \quad (2.1)$$

where R_i is the net rate of production species i by chemical reaction and S_i is the rate of creation by additional from the dispersed plus any user defined sources. The FLUENT by default uses the dilute approximation to model the mass diffusion, which the diffusion flux J_i is written in the following form:

$$J_i = -\left(\rho D_{i,m} + \frac{\mu_t}{Sc_t}\right) \nabla Y_i \quad (2.2)$$

where $D_{i,m}$ is the mass diffusion coefficient for species i , Sc_t is the turbulent Schmidt number and the μ_t turbulent viscosity.

2.4.2 Energy Equation

For low-speed flow inside combustor ($M_a < 0.3$), the energy is shown below:

$$\frac{\partial}{\partial t}(\rho h) + \nabla \cdot (\rho U h) = \nabla \cdot (k \nabla T) + S_h + S_{rad} \quad (2.3)$$

where k is the thermal conductivity and T is the temperature. For ideal gas and incompressible fluid,

$$dh = c_p dT \quad (2.4)$$

So that the equation may be written as

$$\frac{\partial}{\partial t}(\rho h) + \nabla \cdot (\rho U h) = \nabla \cdot \left(\frac{k}{c_p} \nabla h \right) + S_h + S_{rad} \quad (2.5)$$

where S_{rad} is the radiative source term and S_h is the chemical source term where S_h is,

$$S_h = - \sum_j \frac{h_j^0}{M_j} R_j \quad (2.6)$$

where h_j^0 is the enthalpy of formation of species j and R_j is the volumetric rate of creation of species j .

2.4.3 Eddy-Dissipation Model

In the eddy-dissipation model, the reaction rate is controlled by turbulent mixing. The chemical reaction in a combustor is assumed to be very fast; thus, the effect of chemical kinetic is negligible. In ANSYS FLUENT, two values, the reactant R and one for any species P , are calculated as the species production net rate, $R_{i,r}$. The chemical sources term and enthalpy are calculated by the smaller number of two values.

$$R_{i,r} = v'_{i,r} M_{w,i} A \rho \frac{\varepsilon}{k} \frac{\min\left(\frac{Y_R}{v R M_{w,R}}\right)}{R} \quad (2.7)$$

$$R_{i,r} = v'_{i,r} M_{w,i} B \rho \frac{\varepsilon}{k} \frac{\min\left(\frac{\sum_p Y_p}{\sum_j^N v''_{j,r} M_{w,j}}\right)}{R}$$

where A and B are set by default with a value of 4.0 and 2.0, respectively. The eddy-dissipation model and the rate of $R_{i,r}$ are based on the turbulent time scale k/ε , it tends to overestimate the production rate. So, in the CFD simulation, the overall temperature predicted is often higher compared to experimental data. But this issue can be overcome by tuning the empirical constant.

2.4.4 Standard $k - \varepsilon$ model

The standard $k - \varepsilon$ model is a semi-empirical model proposed by Launder & Spalding (1972). The turbulence kinetic energy k and the rate of dissipation ε are obtained from the transport equations (2.8) and (2.9).

$$\frac{\partial}{\partial t}(\rho k) + \frac{\partial}{\partial x_i}(\rho k u_i) = \frac{\partial}{\partial x_j} \left[\left(\mu + \frac{\mu_t}{\sigma_k} \right) \frac{\partial k}{\partial x_j} \right] + G_k + G_b - \rho \varepsilon - Y_M + S_k \quad (2.8)$$

$$\begin{aligned} & \frac{\partial}{\partial t}(\rho \varepsilon) + \frac{\partial}{\partial x_i}(\rho \varepsilon u_i) \\ &= \frac{\partial}{\partial x_j} \left[\left(\mu + \frac{\mu_t}{\sigma_\varepsilon} \right) \frac{\partial \varepsilon}{\partial x_j} \right] + C_{1\varepsilon} \frac{\varepsilon}{k} (G_k + C_{3\varepsilon} G_b) - C_{2\varepsilon} \rho \frac{\varepsilon^2}{k} + S_\varepsilon \end{aligned} \quad (2.9)$$

where G_k is the generation of turbulence kinetic energy due to mean velocity gradients, G_b is the generation of turbulence kinetic energy due to buoyancy, Y_M is the contribution of the fluctuating dilatation in compressible turbulence to the overall dissipation rate, S_k and S_ε are the user-defined source terms, $C_{1\varepsilon}$, $C_{2\varepsilon}$, and $C_{3\varepsilon}$ are constants, σ_k and σ_ε are the turbulent Prandtl numbers for k and ε .

2.4.5 Standard $k - \omega$ model

The standard $k - \omega$ model is an empirical model based on model transport equations (2.10) and (2.11) for the turbulence kinetic energy k and the specific rate of dissipation ω (Wilcox, 1998).

$$\frac{\partial}{\partial t}(\rho k) + \frac{\partial}{\partial x_i}(\rho k u_i) = \frac{\partial}{\partial x_j} \left(\Gamma_k \frac{\partial k}{\partial x_j} \right) + G_k - Y_k + S_k \quad (2.10)$$

$$\frac{\partial}{\partial t}(\rho \omega) + \frac{\partial}{\partial x_i}(\rho \omega u_i) = \frac{\partial}{\partial x_j} \left(\Gamma_\omega \frac{\partial \omega}{\partial x_j} \right) + G_\omega - Y_\omega + S_\omega \quad (2.11)$$

where G_k is the generation of turbulence kinetic energy due to mean velocity gradients, G_ω is the generation of specific dissipation rate, S_k and S_ω are user-defined source terms, Y_k and Y_ω are the dissipation of k and ω due to turbulence, Γ_k and Γ_ω are the effective diffusivity of k and ω , respectively.

2.4.6 Shear-Stress Transport (SST) $k - \omega$ model

Menter (1994) developed the shear-stress transport (SST) $k - \omega$ model. This model combines the robust and accurate formulation of the $k - \omega$ model in the near-wall region with the free stream independence of the $k - \varepsilon$ model in the far field. The transport equations for the SST $k - \omega$ model is written as follow,

$$\frac{\partial}{\partial t}(\rho k) + \frac{\partial}{\partial x_i}(\rho k u_i) = \frac{\partial}{\partial x_j} \left(\Gamma_k \frac{\partial k}{\partial x_j} \right) + \widetilde{G}_k - Y_k + S_k \quad (2.12)$$

$$\frac{\partial}{\partial t}(\rho \omega) + \frac{\partial}{\partial x_j}(\rho \omega u_j) = \frac{\partial}{\partial x_j} \left(\Gamma_\omega \frac{\partial \omega}{\partial x_j} \right) + G_\omega - Y_\omega + D_\omega + S_\omega \quad (2.13)$$

where \widetilde{G}_k is the generation of turbulence kinetic energy due to mean velocity gradients, calculated from G_k , and D_ω is the cross-diffusion form.

2.4.7 Selection of turbulence model

The turbulence standard $k - \varepsilon$ model is chosen as this model characterizes turbulent combustor flow very well, and it is widely applied in the preliminary combustor design system. Besides, this model is robust and economical, and it shows satisfactory accuracy for a wide range of turbulent flows (Fluent Ansys, 2013). Hence, it is commonly used in simulations of industrial flow and heat transfer. The assumption made in the derivation of this model is that the flow is fully turbulent, and the effects of molecular viscosity are insignificant. Thus, this model is compatible for fully turbulent flows. While the combustion model used is the species transport because it predicts the transport and mass fraction of the species, which will be helpful in observing the mass fraction of the specific species. (Pegemanyfar and Pfitzner, 2006)

2.5 Fluid-Structure Interaction

There are various methods available for FSI simulation. The selection of a particular method generally depends on the availability of the fluid and solids solver code, computation time, and the importance of the solid deformation process to the physics involved (Patil *et al.*, 2015).

(Ha *et al.*, 2017) remarked that the numerical approaches used in FSI could be categorized into two groups: monolithic approach and partitioned approach. (Benra *et al.*,

2011) stated that partitioned methods are divided into one-way and two-way coupling, subdivided into weakly and strongly coupled methods.

ANSYS alleged that some cases only require one-way coupling or known as direct coupling. For example, deflection of the geometry caused by the pressure loadings changes the flow field around the geometry, but the change is negligible since it is a minor change. Thus, it is unnecessary to adjust the geometries back in the fluid solver and rerun the simulation. This method usually involves the unidirectional fields interaction and is solved directly in a single solution.

(Roul and Kumar, 2020) modeled the structure and fluid to understand better the high structure reaction and vibration of the turbine blade. They applied the FEA and CFD approach to perform the structural analysis on the turbine blade. One-way FSI is used to investigate the performance parameter, which is the deformation and the Von-mises stress acting on the turbine blade. The results show the favourable pitch angle is critical to building an optimized turbine blade that can reduce the strength of the unsteady load without significant power loss.

(Badshah, Badshah and Kadir, 2018) Also carried out a similar study on the turbine blade to evaluate the structural load characterization under profiled and uniform flow by utilizing the ANSYS. The results indicate that the turbine blade was subjected to deformation and uniform stress when the turbine rotates in a uniform flow, leading to fatigue failure.

2.6 Research Gap

Based on the literature review, most researchers only focus on the blade of the turbine engine and combustion performance by altering the geometry parameter. Besides, this chapter has shown many researchers also carried out simulation studies on aero-

engine combustors. But these researches are more focused on combustion fluid flow and heat transfer characteristics of the combustor liner related to combustion simulation. Typically, the fuel used was just only one type because the geometry parameter is the primary manipulation variable.

Other than that, the failure analyses of the combustor and the turbine blade are performed chiefly from the point of view of the material detection, which to identify the failure mode. But it is still challenging to identify the influencing factor, such as the stress and strain on the failure of the combustor, as it can be beneficial for the service life assessment and strength design of the combustor.

So, it is essential to mention that the influence of the combustion characteristics of the fuels on the combustor mechanical properties is scarcely taken into account. In other words, it is to say, the relationship between the performances of the fuels and mechanical properties of the combustor is still imprecise.

This research will focus on the combustion of the four different fuels, Ethanol, Biodiesel, CSPK, and Jet-A, mainly to study the difference in combustion performance, temperature distribution, and subsequently the effect of the thermal stress on the combustor casing by using one-way FSI in the hope of giving future researchers some new and clear insight into developing the gas turbine combustor.

CHAPTER 3

METHODOLOGY

3.1 Overview

This chapter discusses the methods to carry out the project in detail.

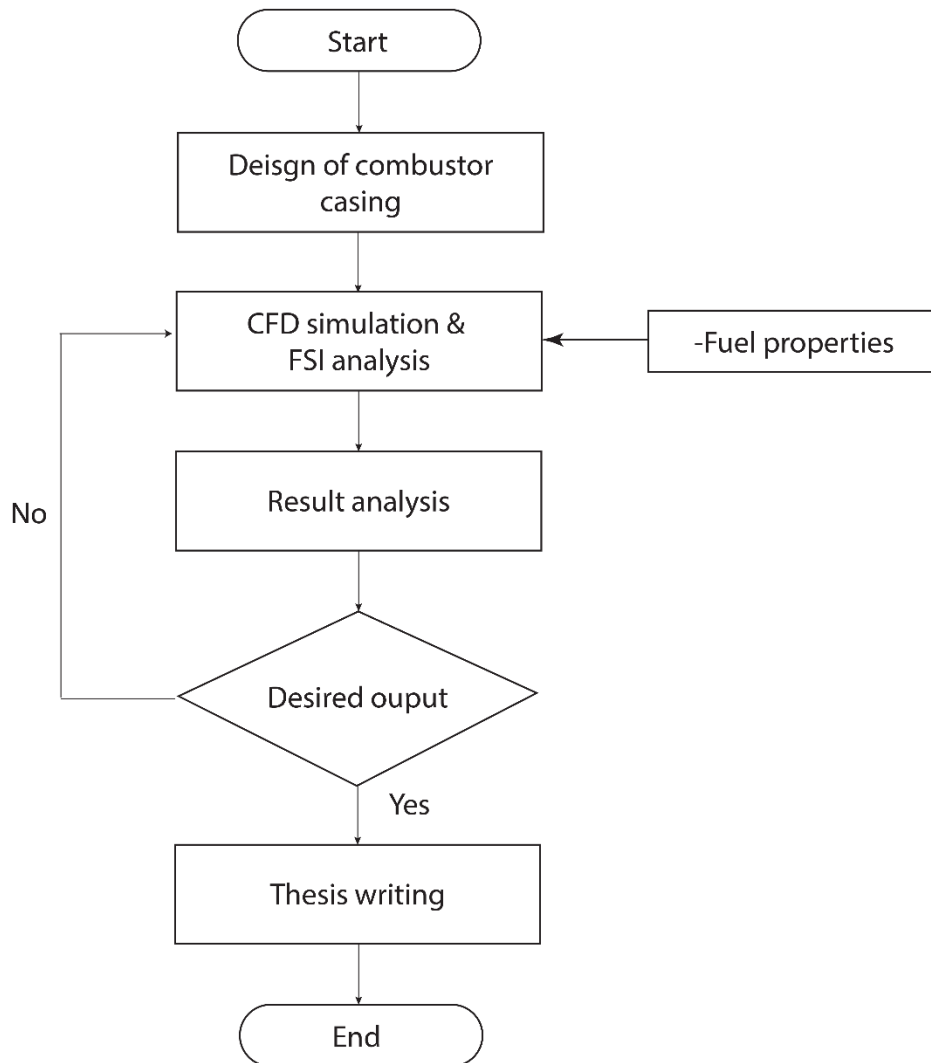


Figure 3.1: General flowchart of this research

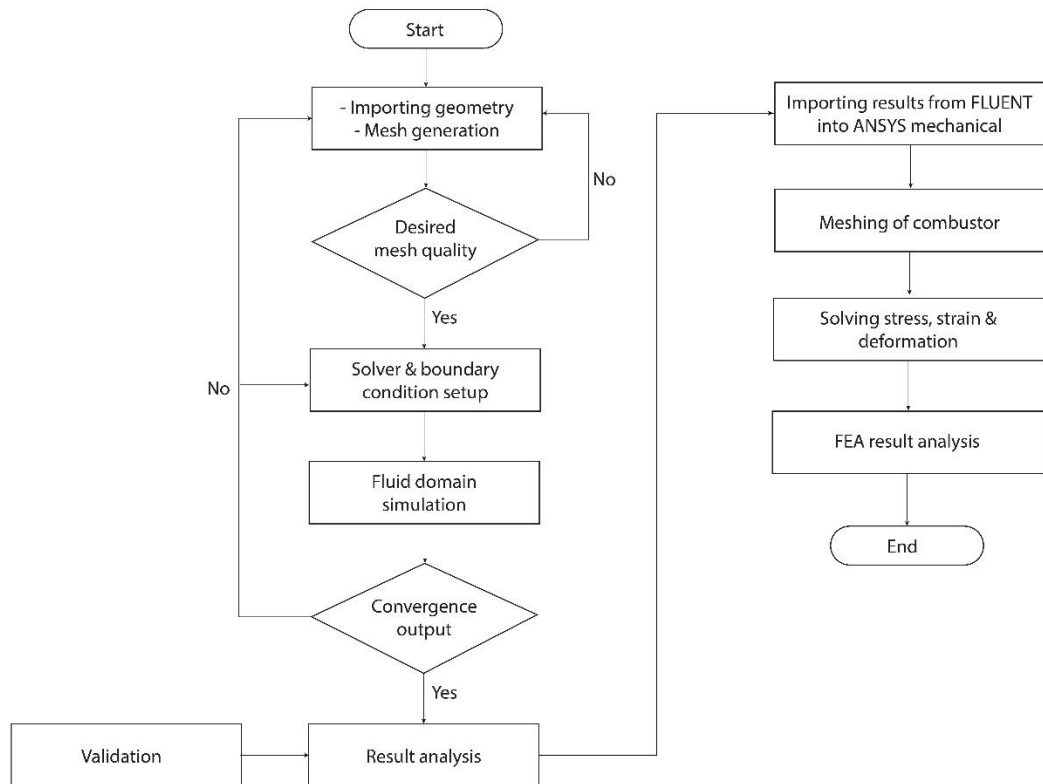


Figure 3.2: Detailed flowchart for simulation process

3.2 Geometry Selection of combustor

Generally, tubular, annular, and tuboannular are the three main types of combustor. But the most used type of combustor is the annular combustor because it has quite a few advantages, including the shorter length of the liner, and tends to have uniform combustion distribution and exit temperature.

However, this study will focus entirely on the tubular combustor to discover more about the combustion behavior through geometry design as the simulation can be performed by just considering one combustor can instead of all. (Conrado *et al.*, 2004) discussed the design methodology, in the primary stage of this work, the designing process will be presented through a simpler and transparent approach to reduce the

development time and give plenty of time at the refining phase. Generally, this section will be discussing the flow of the geometry determination and equations used.

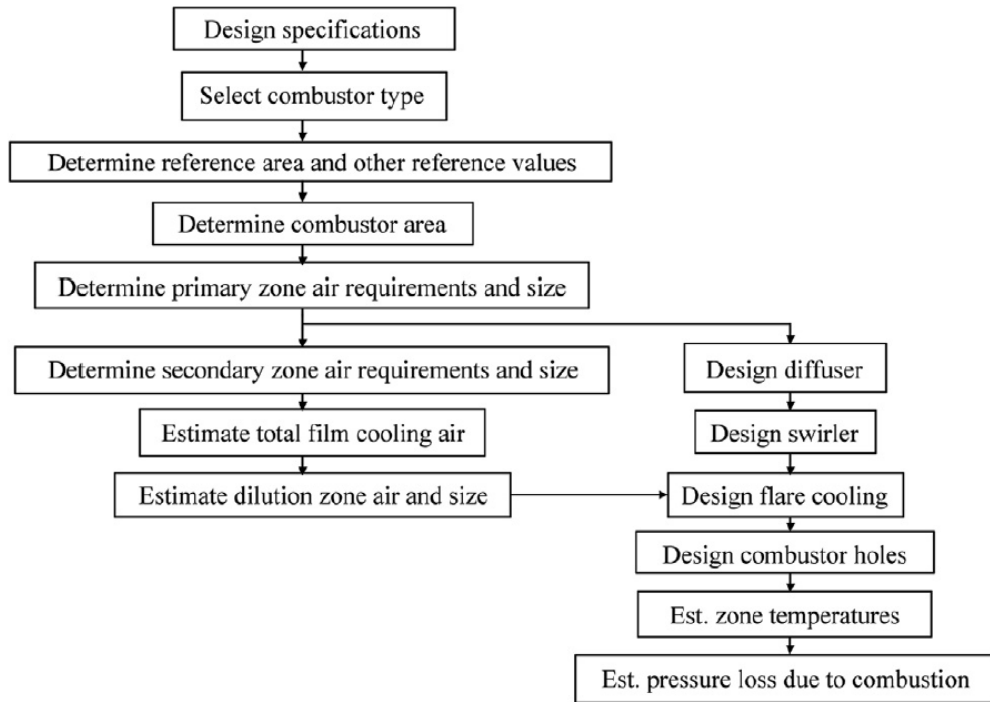


Figure 3.3: Preliminary design procedure of the combustor (Mark and Selwyn, 2016)

To emphasize, the reference area is one of the most important design parameters of a combustor as it is an impactful parameter to other dimensions. The reference area can be determined by two approaches, based on aerodynamic and combustion process. But the coverage of this work will only include the aerodynamic approach for the reference area calculation to ease the designing process.

So, the reference area is calculated with the following equation,

$$A_{ref} = \left[\frac{R}{2} \left(\frac{\dot{m}_3 \sqrt{T_3}}{P_3} \right)^2 \frac{\Delta P_{3-4}}{q_{ref}} \left(\frac{\Delta P_{3-4}}{P_3} \right)^{-1} \right]^{0.5} \quad (3.1)$$

where $R = 143.5 \text{ J kg}^{-1} \text{ K}^{-1}$

The total pressure loss $\Delta P_{3-4}/P_3$ used in equation (3.1) is a corresponding design value, typically a fixed value which the pressure loss throughout the combustor. While $\Delta P_{3-4}/q_{ref}$ is the function of the pattern factor. Finally, $\dot{m}_3\sqrt{T_3}/(P_3A_{ref})$ is a parameter that varies accordingly with the reference area. Anyway, the detailed calculation of the parameter is not feasible. So, the data presented by (Lefebvre, 2010) will be used for the reference area calculation when the equation (3.1) is used. The data is shown in the following table. Table 3.2 shows the operating condition to be used in the calculation process.

Table 3.1: Typical values used in combustor

Type of chamber	$\frac{\Delta P_{3-4}}{P_3}$	$\frac{\Delta P_{3-4}}{q_{ref}}$	$\frac{\dot{m}_3\sqrt{T_3}}{P_3A_{ref}}$
Tubular	0.07	37	0.0036
Annular-tube	0.06	28	0.0039
Annular	0.06	20	0.0046

Table 3.2: Operating condition for calculation process and simulation (Luis Goular Dias, Antonio Rosa do Nascimento and de Oliveira Rodrigues, 2014)

Parameter	Value	Unit
Air mass flow rate	4.288	kg/s
Inlet air temperature	461.0	K
Air inlet total pressure	405.3	kPa
Air inlet static pressure	389.9	kPa
Fuel mass flow rate	0.745	kg/s
Inlet fuel temperature	430.0	K
Fuel inlet total pressure	405.3	kPa
Fuel injection velocity	15.0	m/s

Pressure loss	6.0	%
Combustion efficiency	0.99	-

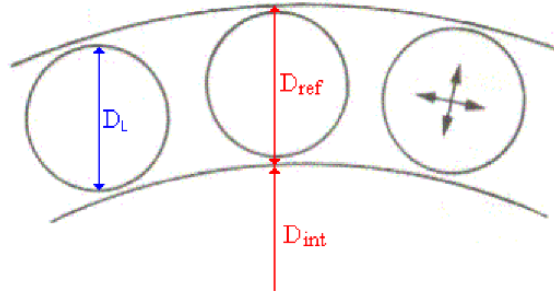


Figure 3.4: Reference length D_{ref} for tubular combustor (Conrado *et al.*, 2004)

The equations shown will below are the equations used to calculate the dimensions of the combustor.

3.2.1 Casing Area

Liner area,

$$A_L = 0.7A_{ref} \quad (3.1)$$

Diameter from the reference area,

$$D_{ref} = \sqrt{\frac{4A_{ref}}{\pi}} \quad (3.2)$$

Diameter from the liner area,

$$D_L = \sqrt{\frac{4A_L}{\pi}} \quad (3.3)$$

Annular area,

$$A_{an} = A_{ref} - A_L \quad (3.4)$$

Pattern factor,

$$PF = \frac{T_{max} - T_4}{T_4 - T_3} \quad (3.5)$$

where T_{max} is maximum exit temperature.

Liner length,

$$L_L = \frac{-D_L}{0.05 \left(\frac{\Delta P_{3-4}}{q_{ref}} \right) \ln(1 - PF)} \quad (3.6)$$

Primary zone length,

$$L_{PZ} = \frac{3}{4} D_L \quad (3.7)$$

Secondary zone length,

$$L_{SZ} = \frac{1}{2} D_L \quad (3.8)$$

Dilution zone length,

$$L_{DZ} = D_L (3.83 - 11.83PF + 13.4PF^2) \quad (3.9)$$

3.2.2 Diffuser Dimension

Snout outer area,

$$A_o = \frac{\dot{m}_3}{\dot{m}_{an}} A_{an} \quad (3.10)$$

where \dot{m}_3 is inlet air mass flow rate and \dot{m}_{an} is the annulus air mass flow rate

Snout outer diameter,

$$D_o = \sqrt{\frac{4A_o}{\pi}} \quad (3.11)$$

Diffuser angle,

$$\varphi = \tan^{-1} \left[\frac{\left(\frac{\Delta P_{3-4}}{q_{ref}} \right) A_3^2 P_3^2}{502.4 \left(1 - \frac{A_3}{A_0} \right)^2 \dot{m}_3^2 T_3} \right]^{1/1.22} \quad (3.12)$$

Diffuser length,

$$L_{dif} = \frac{(R_o - R_3)}{\tan \varphi} \quad (3.13)$$

where R_o and R_3 (inlet radius) are $D_o/2$ and $D_3/2$ respectively

3.2.3 Swirler Dimensions

Snout area,

$$A_s = A_o \frac{\dot{m}_{RZ}}{\dot{m}_3} \frac{1}{C_{ds}} \quad (3.14)$$

where \dot{m}_{RZ} is the recirculation zone mass flow inlet and C_{ds} is the snout discharge coefficient (for an uniform compressor delivery, it is unity)

Snout diameter,

$$D_s = \sqrt{\frac{4A_s}{\pi}} \quad (3.15)$$

Swirler flow area,

$$A_{sw} = \frac{A_{ref}^2}{\sqrt{\left[\frac{\Delta P_{sw}}{q_{ref}} \left(\frac{\dot{m}_3}{\dot{m}_{sw}} \right)^2 + \left(\frac{A_{ref}}{A_L} \right)^2 \right] \cos^2 \beta_{sw}}} \quad (3.16)$$

where K_{sw} is the concordance factor (1.30 for thin straight blades) and β_{sw} is the turning angle (45° for this project)

Swirler diameter,

$$D_{sw} = \sqrt{\left[\frac{A_{sw}}{n_B} + \left(\frac{\pi}{4} D_{hub}^2 \right) \right] \frac{4}{\pi}} \quad (3.17)$$

where D_{hub} is injector hub diameter and n_B is the number of swirler blades.

3.2.4 Recirculation Zone Dimensions

Recirculation zone length,

$$L_{RZ} = 2D_{sw} \quad (3.18)$$

Recirculation zone angle,

$$\theta_{RZ} = \cos^{-1} \left[\frac{-D_L(D_L - 2D_{sw}) - (D_L - 4L_{RZ}) \sqrt{D_L^2 - 4D_L D_{sw} + 4D_{sw}^2 - 8D_L L_{RZ} + 16L_{RZ}^2}}{2D_L^2 - 4D_L D_{sw} + 4D_{sw}^2 - 8D_L L_{RZ} + 16L_{RZ}^2} \right] \quad (3.19)$$

Dome length,

$$L_{dome} = \frac{D_L - D_{sw}}{2 \tan \theta_{RZ}} \quad (3.20)$$

3.3 Fluid Domain Solver Setup

The solver chosen is the pressure-based steady-state with the energy equation checked. The turbulence model used is the standard $k - \epsilon$ model with the standard wall function. The Species Transport with Eddy Dissipation model is used for the combustion process. The Eddy Dissipation model was chosen because it is a general model and considers, among other factors, turbulent burning, and diffuse flames. Besides, the P1 radiation model is used to calculate the radiation heat transfer because the P1 model works well under combustion applications where the optical thickness is large. Also, the P1 model can easily be applied and is suitable for complex geometries. The simulation is then performed by using the commercial code ANSYS FLUENT. Table 3.3 and Table 3.4 show the fuel properties and the solver setup.

Table 3.3: Fuel Properties

Fuel Properties	Jet A	CSPK	Biodiesel	Ethanol
Specific heat (J/kgK)	2093	2177.36	1398.23	2570
Molecular formula	$C_{12}H_{23}$	$C_{12}H_{25.4}$	$C_{17}H_{34}O_2$	C_2H_5OH
Density (kg/m ³)	780	749	874.9	789.45
Viscosity (cST)	8.0	3.663	4.546	3.806
Low Heating Value (MJ/kg)	42.8	44.0	37.8	26.7
Boiling point (K)	449	248	478	349

Table 3.4: Solver setup and boundary condition

Properties	
Energy equation	On
Viscous model	k-epsilon
Wall treatment	Standard
Radiation model	P1